Full Text View

Volume 29, Issue 11 (November 1999)

Journal of Physical Oceanography
Article: pp. 2962–2970 | Abstract | PDF (158K)

Convective Mixing and the Thermohaline Circulation

Jochem Marotzke and Jeffery R. Scott

Center for Global Change Science, Massachusetts Institute of Technology, Cambridge, Massachusetts

(Manuscript received June 1, 1998, in final form January 29, 1999)

DOI: 10.1175/1520-0485(1999)029<2962:CMATTC>2.0.CO;2

ABSTRACT

An idealized three-dimensional model of buoyancy-driven flow in a single hemisphere is used to investigate the relationship between the meridional overturning and the efficiency by which convective mixing eliminates static instability. In the “fast” limit (mixing timescale hours to weeks), the meridional overturning is not rate limited by the efficiency of convective mixing. If convective mixing is made less efficient, the model’s meridional overturning strength *increases.* Moreover, the dominant downwelling occurs not at the highest surface density;hence the deep ocean is relatively buoyant. The numerical results are explained by the different influences of convective mixing and downward advection on the deep-ocean heat budget; they underscore the fundamentally three-dimensional nature of the meridional overturning. In addition, the narrowness of deep downwelling is related to the geostrophic dynamics of deep temperature anomalies near the eastern wall. The model results presented here are in contrast to the expectation that deep-water formation by convective mixing is a necessary, if not rate-limiting, ingredient to the existence of a thermohaline circulation.

1. Introduction

The prevailing conceptual picture of the thermohaline circulation (THC) comprises a highly localized, downward, convective branch and a broad upwelling branch. However, the connection between convective activity and the large-scale flows is not straightforward. The integral (regional scale) effect of open-ocean deep convection is best characterized as vigorous mixing without net vertical mass transport (Send and Marshall 1993; Klinger et al. 1996). As a consequence of the water mass modifications by convective mixing, zonal-mean zonal density and pressure gradients are such that near-surface meridional transport is toward the latitude of convection, and deep transport is away from it (Marotzke 1997, hereafter M97). The vertical motion then arises from mass continuity of the divergent horizontal transport. The violent *convective mixing* and the *downwelling* are two fundamentally different processes, yet they are frequently considered synonymous. To elucidate their relationship is one

focus of this paper.

In steady state, the convective vertical buoyancy transfer is balanced by buoyancy loss to the atmosphere, and upward advection into the pycnocline is balanced by downward or, more precisely, diapycnal diffusion (Munk 1966). Notice that two very different vertical mixing processes are involved: Convective mixing reduces the potential energy of the water column (the center of mass is lowered), while diapycnal mixing in stratified water increases the potential energy (Weyl 1968) and hence requires a source of mechanical energy (Huang 1998; Munk and Wunsch 1998). Also, notice that in order to "tap" the reservoir of potential energy,[1] there must be a dynamical mechanism to convert the potential into kinetic energy, such as geostrophic adjustment induced by tilted isopycnals.

The question frequently arises (see, e.g., the last paragraph in the review of Marshall and Schott 1999) whether one should consider the meridional overturning circulation resulting from the mixing processes as being "pushed" down by convection or "pulled" up by the downward diffusion. It is clear that the question must be refined: Both convective mixing and vertical diffusion are commonly considered essential elements of the THC; since they balance in steady state, causality is not readily established. There is, however, a straightforward—albeit to our knowledge hitherto unused—way of making the question answerable. One can ask whether the strength of the THC is controlled by the diapycnal or by the convective mixing. Depending on whether the first or the second process is rate limiting, one would be entitled to call the THC pulled or pushed. Numerous numerical modeling studies have shown that the THC strength increases with diapycnal diffusivity (e.g., Bryan 1987; Colin de Verdière 1988; M97), but no corresponding study has been performed, varying the efficiency of convective mixing.[2] Here, we describe idealized numerical experiments in which this is done. First, convective efficiency is varied within a "realistic" range so that removal of instability occurs on a timescale faster than any other important timescale in the model. Next, convective mixing is assumed unrealistically slow: while not necessarily meant to simulate a realizable flow, this should teach us something fundamental about the role of convective mixing in buoyancy-driven flow. During this exploration, we are naturally led back to the old question of why deep sinking in the ocean is narrow (Stommel 1962; Rossby 1965; Winton 1995). We show that previously given explanations are incomplete when three-dimensional rotating dynamics apply.

2. Model description

The model is identical to the one used in M97. It is the Geophysical Fluid Dynamics Laboratory (GFDL) primitive equation GCM, based on the method described in Bryan (1969) in the version documented and distributed by Cox (1984). The domain extends from the equator to 64°N and is 60° wide; the bottom is at a constant depth of 4500 m. Horizontal resolution is 3.75° zonally by 4° meridionally. There are 15 levels in the vertical, varying smoothly in spacing from 50 m near the surface to 500 m at depth. The model is forced by restoring boundary conditions on both surface temperature and salinity; the target profiles are independent of longitude and vary like the cosine of latitude, with peak-to-peak amplitudes of 27°C and 1.5 psu. The restoring timescale is 30 days, which means that surface temperature and salinity, hence density, are very nearly prescribed. Throughout this paper, "temperature" and "buoyancy" will be used synonymously. Surface wind stress is set to zero. Asynchronous integration is used (Bryan 1984), with a temperature and salinity time step of 5 days and a momentum and vorticity time step of 2 hours. Standard horizontal and vertical friction parameterizations are used with coefficients 2.5×10^5 m^2 s^{-1} and 10^{-2} m^2 s^{-1}, respectively; horizontal diffusivity is set to 10^3 m^2 s^{-1}. Within one grid cell of the perimeter of the basin, vertical diffusivity k_υ is 5×10^{-4} m^2 s^{-1}, uniformly with depth; otherwise, k_υ is zero under statically stable conditions. This spatial distribution of k_υ reflects in a crude way that mixing occurs primarily near the ocean margins (Munk 1966; Wunsch 1970; Armi 1978; Polzin et al. 1997).

Static instability is removed by a convective adjustment procedure in which the vertical diffusivity is increased to a very high value where denser water is above lighter water. It is this parameterization of convection that allows us to test its efficiency in a very well defined way. The value of the "convective diffusivity," k_c, was 1 m^2 s^{-1} in M97. Here, it is varied between 10 m^2 s^{-1} and 5×10^{-4} m^2 s^{-1}.

3. Numerical results

a. The "fast" convection limit

The value of the "convective diffusivity" k_c is set to 10, 1, and 0.1 m^2 s^{-1} in experiments 1, 2, and 3, respectively. Klinger et al. (1996) inferred from their nonhydrostatic, three-dimensional numerical experiments that convection is adequately parameterized by $k_c = 10$ m^2 s^{-1}, which corresponds to a mixing timescale of about 1 day over a depth of 1 km. Hence, the k_c values in experiments 2 and 3 are low compared to realistic convection situations, but they put the model into

the "fast " or "efficient" convective mixing regime.[3] Figure 1 shows the meridional overturning circulations of experiments 1, 2, and 3. There is virtually no difference between the solutions; the maximum overturning values are 19.13 Sv, 19.18 Sv, and 19.49 Sv in experiments 1, 2, and 3, respectively (Sv $\equiv 10^6$ m^3 s^{-1}). So, varying the efficiency of convection by two orders of magnitude leads to a change in overturning of about 1.5%. In contrast, changing the vertical diffusivity in stratified waters by two orders of magnitude led to a change by a factor of 6 in experiments similar to those of M97 (J. Scott 1998, unpublished results).

Notice that the situation described here is analogous to that in the atmosphere, where the amount of radiative cooling, not convection, limits the strength of the Hadley circulation (Emanuel et al. 1994). Notice also that the rate-limiting role of diapycnal mixing applies to the global integral of the THC, not to the individual sources of deep water (Tziperman 1997; Klinger and Marotzke 1999; Marotzke and Klinger 2000). For example, changes in convection in the Labrador and Greenland Seas would influence the Atlantic overturning cell. Concerning the global integral of deep-water formation, however, the diapycnal but not the convective mixing is the rate-limiting factor, so in the "fast" convection limit one can loosely say that the thermohaline circulation is "pulled up," not "pushed down."

b. Inefficient convective mixing

While the results from the previous subsection give a simple and unambiguous interpretation, it is of interest to see how far k_c must be lowered before it does make a difference; this would mark the boundary of the fast convection limit. Clearly, the expectation is that weaker convective mixing leads to weaker meridional overturning. In experiments 4, 5, and 6, k_c is reduced further to 100, 10, and 5 ($\times 10^{-4}$ m^2 s^{-1}) respectively. While it is extremely unlikely that a system with k_c so low is physically realizable, we consider it a problem in geophysical fluid dynamics, trying to understand the role of convective mixing by making it artificially small.

Figure 2 shows that as k_c is lowered, the sinking rate does not decrease, but rather increases monotonically to almost 50 Sv in experiment 6 ($k_c = 5 \times 10^{-4}$ m^2 s^{-1}). Moreover, the downwelling latitude moves away from the northern wall as k_c is reduced and is located at 48°N in experiment 6. There is no longer a single overturning cell, but the downwelling is distributed over a thermally direct cell at low and middle latitudes and a thermally indirect cell at higher latitudes. Experiments 1 through 6 show that a change in convective mixing coefficient k_c over four orders of magnitude leads to a change in overturning of less than a factor of 3. (Notice that even in expts 1–3, a *decrease* in k_c leads to an *increase* in overturning, albeit a small one.)

The increase in circulation is surprising and raises a number of fundamental questions about the roles of convective mixing, downwelling, and their relationships with geostrophic force balance. The next subsection will address these questions by comparing solutions of experiments 2 and 6 (see M97; expt 2 here was his standard run); the discussion section will put the results into a larger context.

c. Three-dimensional dynamics

The difference between experiments 2 and 6 (Figs. 1b and 2c, respectively) is now explained by looking at salient three-dimensional features. Figure 3a shows temperature of experiment 6 at 425-m depth. Almost the entire meridional gradient is concentrated in the front centered around 48°N, leading to a vigorous and narrow eastward near-surface current and a corresponding vigorous downwelling (not shown) as this flow hits the wall. The temperature section along the eastern wall (Fig. 3b) shows that the downwelling is strong enough to virtually homogenize the water column, thus setting the very high deep-ocean temperatures, which are around 7°–8°C. The effect of the downwelling on bottom-layer flow and temperature is clearly seen in Figs. 3c and 3d, respectively. Water is injected into the deep layer at the eastern boundary at 48°N, moves westward in thermal wind balance with the front, and fans out northward and southward.

The downwelling region at the eastern wall is two grid cells wide, meridionally, reflecting that the eastward surface current leads to downwelling in the two neighboring temperature grid points. If the resolution were higher, the width of the front would be determined by more physical causes, but would still be finite. Owing to the nearly fixed meridional surface temperature gradient, the downwelling columns carry water of different temperatures. Since the horizontally averaged bottom layer temperature is roughly the average temperature of the two downwelling branches, the northern branch is cold relative to the surroundings while the southern branch is warm. This is clearly visible in the temperature dipole in Fig. 3d, near the eastern wall and near 48°N; the dipole represents both the coldest and the warmest bottom temperatures.

From thermal wind, the deep circulation is clockwise around a temperature minimum and anticlockwise around a maximum (notice that there is no wind forcing, so the vertically integrated horizontal velocity is zero, and we can safely

assume a middepth level of no motion). As one consequence, maximum deep upward velocities along the eastern wall are right next to the region of maximum downwelling (not shown). The meridional overturning is balanced by the density difference between eastern and western walls (see M97 for a detailed discussion); the upwelling pattern leads to relatively cold (warm) water at the eastern wall north (south) of 48°N. Again assuming a middepth level of no motion, this balances relatively vigorous vertical shear in deep meridional flow, southward south of 48°N and northward north of 48°N, as displayed in the meridional overturning (Fig. 2c). To close the logical sequence, notice that the two counterrotating overturning cells converge at 48°N, which establishes the sharp front there.

If convective mixing to the bottom is present, we expect the convective cooling to have a major impact on the bottom-layer heat budget. By modifying the argument above, we expect that horizontally averaged deep temperature is an average of the convecting water (the coldest deep temperatures, which occur in the northwestern corner, Fig. 4) and the downwelling water. While the latter still brings waters of different temperatures to the bottom layer, this difference is less important since a heat sink is present by the convective cooling. Hence, a warm anomaly is created at the downwelling site, with associate counterclockwise deep flow (Fig. 6b of M97) and, again, very large upwelling just south of the maximum downwelling (shown in Fig. 3c of M97 but not explained). We see that the very unrealistic experiment 6 helps explain an important feature of experiment 2, while, conversely, experiment 2 helps explain how "switching off" convection moves the downwelling site southward. When convective mixing is strong, the main deep heat balance is between the convective cooling and the warm (southern) branch of the downwelling; the cold (northern) branch of the downwelling is close to the averaged deep temperature and hence not very conspicuous (Fig. 4). When convective mixing is no longer available to provide a heat sink for the deepest layer, this role must be taken over by the cold branch of the downwelling. As the cold anomaly becomes more pronounced (Fig. 3d), so does the associated vortex, which "moves" southward pushing the warm vortex along. As one consequence of the southward "migration," the aforementioned upwelling at the eastern wall occurs in more stratified water, and one would expect a stronger effect on density. Indeed, the increase in overturning strength (cf. Figs. 2c and 1b) is in large part due to the increase of thermal wind shear at depth, while the thermocline zonal-mean zonal density difference is similar between the two experiments (figure not shown).

4. Discussion

Open-ocean deep convection is not directly associated with a net vertical mass transport (Send and Marshall 1993; Klinger et al. 1996), yet there is considerable downwelling in the northern North Atlantic, as determined from mass continuity (e.g., Macdonald and Wunsch 1996), which begs the question of *where* the sinking occurs. While knowledge of the horizontal flow convergences is not good enough to provide detailed answers for the real ocean, some general statements can be made.

a. Three-dimensional versus two-dimensional dynamics

In two-dimensional ocean models, the downwelling occurs at the convection site since most of these models (e.g., Marotzke et al. 1988; Wright and Stocker 1991; Cessi and Young 1992; Thual and McWilliams 1992; Quon and Ghil 1992) assume a local and linear balance between the meridional pressure (hence density) gradient and the flow strength (Wright et al. 1995 seem to be the only exception in using nonlocal dynamics). Convective mixing to the bottom occurs at the location of highest surface density, which has the lowest sea level and hence is a convergence point of surface flow. Notice that this situation does not change if convective mixing is turned off. The downwelling still occurs at the same location, and there is little change in the steady-state solutions under fixed surface density, with or without convective mixing (as shown by Marotzke et al. 1988).

Zhang et al. (1992) noted the fundamental difference between two- and three-dimensional models, concerning the importance of convective mixing. When they turned off convective adjustment in their three-dimensional model, sinking to the bottom occurred at the latitude of maximum Ekman pumping (Zhang et al. 1992, p. 113). As the experiments presented here demonstrate, vigorous downwelling even persists under pure buoyancy forcing. (Consistently, Zhang et al. 1992 stated that wind forcing was not required in the reversal of their high-latitude overturning; they did not, however, show results from a run with both wind and convection turned off.) In three dimensions, the location of maximum surface density and hence of convective mixing to the bottom need not coincide with the location of strongest downward mass transfer. Indeed, in experiment 2, convective mixing to the bottom occurs in the northwestern corner, while the strongest downwelling (and generally deep mixed layers but not the very deepest convection) occurs in the northeast (see M97; expt 2 here was his standard run). Still, downwelling and the deepest convection occur at the same latitude, in experiment 2, which obviously is not the case any longer as convective mixing becomes inefficient (expt 6).

b. Narrowness of sinking region:[4] Appraisal of early work

Why oceanic sinking is confined to narrow regions was explored by Stommel (1962) through theory and Rossby (1965) by laboratory experiment (Rossby's model was heated from below; the discussion here is in terms of its oceanic equivalent). Later, this question was taken up again by Winton (1995), who pointed out that neither Stommel (1962) in his model of horizontally connected vertical pipes nor Rossby (1965) included turbulent convective mixing as an important ingredient.

Both early works can hence be characterized as dealing with nonrotating, quasi-two-dimensional systems without convective mixing: both show narrow sinking at the location of the lowest surface temperature and broad upwelling everywhere else. The narrowness of sinking is maintained in our three-dimensional experiments, with or without convective mixing, but not necessarily at the coldest surface temperature. This invites the question of exactly what is the physical cause of the narrowness of sinking?

Interestingly, Stommel (1962) provided no qualitative physical explanation at all but merely showed various solutions to his model. Rossby (1965) gave the interpretation that apparently has become standard: In steady state, the ocean is cooled by convection and heated by turbulent mixing; since convection is much more efficient, the area of turbulent mixing must be accordingly larger. However, efficient vertical heat transfer by either convective mixing or vigorous downwelling can explain why the deep ocean has the properties of the convecting or downwelling water but cannot by itself explain why the area of efficient vertical heat transfer is small. Diapycnal mixing acts on a much larger temperature difference than does convective mixing, hence a large vertical transport is possible even if the upwelling region does not span almost the entire ocean. In other words, it is not at all clear why a smaller area for upwelling and downward diffusion (leading to deep-water properties even closer to those of the convecting water) should be unacceptable. Indeed, Stommel (1962) analyzed the case where no diffusive mixing at all reached the deep ocean (assuming incorrectly the existence of a level of vanishing stratification and hence diffusive flux), which consequently had the temperature of the single downwelling pipe. Physically, the reason for the concentration of downwelling in a single pipe is the same as in the two-dimensional models: All flow converges to the point of lowest temperature and hence lowest sea level (unless some intermediate point is much warmer than either of the endpoints; Stommel's large-γ limit, p. 771). Stommel's (1962) and Rossby's (1965) physical discussions hence cannot explain narrow downwelling in three-dimensional systems.

c. Narrowness of sinking region: Energetics

By reworking Stommel's (1962) model with two vertical pipes of differing cross sections and the sum of the cross sections fixed, Winton (1995) made two interesting observations. First, narrow sinking produced the solution that had minimal potential energy since it implied that the sinking water and, hence, the deep ocean had the temperature of the coldest surface point, by token of the two-dimensional dynamics discussed above. A broader sinking region would impart its average temperature onto the deep ocean and make it warmer than in the narrow sinking case. The second observation was that, once the deep ocean temperature was assumed given, wide upwelling meant minimum upwelling velocity, hence maximum downward penetration of the diffusive thermocline, maximum baroclinic pressure gradients, and maximum meridional overturning strength. Winton's (1995) list of extremes can be extended: For given (cold) deep temperatures, wide upwelling leads to the state of maximum available potential energy, of maximum heat transport, and of maximum internal entropy production (which is of the order heat transport × horizontal temperature variation). It is unclear whether these properties of available potential energy or entropy production are coincidental or express something fundamental about the fluid.

Concerning his first observation, Winton (1995) already noted that merely identifying a state of lower potential energy is not sufficient to ensure that it is attained. In his model, this would require narrowing the sinking region—but "moving" the pipes is not part of the fluid dynamical system and hence not accessible as a dynamical path. In contrast, a higher-resolution model has the freedom to narrow the sinking region or to move it toward lower surface temperatures. More generally, the equations governing the fluid must permit the temporal evolution to the state of lower energy. In the two-dimensional models, this evolution is almost trivially guaranteed since the dynamics lead to sinking or convective mixing, or both, at the highest surface density. Hence, the "energy principle" (i.e., the tendency to attain the state of lowest potential energy) does not lead to any new, general statement about the solution. Notice further that under two-dimensional dynamics both convective mixing and downwelling, while being very different processes, have a similar effect on the energetics since both bring the densest water to the bottom. The same does not necessarily hold under three-dimensional dynamics because the downwelling water can have temperatures different from the convecting water (see also the following subsection).

d. Narrowness of sinking region: Three-dimensional dynamics

In three dimensions, the limitations of the energy principle become obvious: there must be a dynamical path to tap the potential energy that rests in the unstable stratification at high latitudes. If this path is provided by efficient convective mixing (lowering the potential energy, see Huang 1998), then indeed the deep ocean is as cold as possible. If, in contrast, convective mixing is inefficient, the state of minimum potential energy, consistent with purely thermodynamic considerations (deep water as cold as, but no water colder than, the coldest surface temperature), cannot be attained. The reason is that the heat balance of the lowest layer in the presence of vigorous concentrated downwelling of small but finite area causes the sinking to be located away from the northern boundary (see section 3). As a consequence, deep water is relatively warm and the potential energy of the steady state relatively high. If one may infer that the available potential energy is likewise higher with inefficient convective mixing [which is plausible according to Huang (1998) but not a forgone conclusion] and, moreover, that the overall level of kinetic energy increases with increasing available potential energy (again plausible but by no means certain), the stronger overturning in experiment 6 above would be logically linked to the higher potential energy. This connection is speculative at this point; exploring it would go beyond the scope of this paper but is a topic worthy of

closer attention.

Finally, we offer an explanation of why deep downwelling is narrow, even under three-dimensional dynamics. Assume that the downwelling along the eastern wall is indeed more widespread. Irrespective of its spatial extent, its equatorward side creates a warm anomaly in the bottom layer, while the poleward side creates a cold anomaly. But a warm anomaly abutting the eastern wall self-propagates northward and a cold anomaly propagates southward, as can be seen by applying the method of images [e.g., Kundu (1990, p. 137) applied here not to point vortices but widespread vorticity anomalies; for the following argument, we make the reasonable assumption that the shallow currents are mainly determined by the surface forcing and shallow density gradients, which show no vortex structures]. To fulfill the no-normal flow sidewall boundary condition, one can assume the warm anomaly, which creates anticlockwise flow at depth, to be under the influence of an image cold anomaly of equal strength and distance from the wall, but on the other side of the boundary. Hence, the real warm anomaly is on the western flank of clockwise flow and advected northward. By the analogous reasoning, the cold anomaly is advected southward. One would expect the temperature extremes at the boundaries of the downwelling region to be strongest in this self-propagation, meaning that they would be pushed toward each other as close as permitted by the spatial resolution or by roughly the deformation radius. With vigorous convective mixing (expt 2), the cold branch of the downwelling region cannot develop a noticeable vortex in an ambient temperature that is determined by an average of deep-mixing water and the warm branch of the downwelling. Hence, the deep warm vortex moves all the way to the northern boundary, becoming as narrow as possible. [These statements must be modified if diapycnal mixing is much stronger than assumed here (J. Scott 1998, unpublished results).]

Notice that the propagation of the warm and cold deep vortices toward each other can also be interpreted through the "convergent boundary wave" mechanism described in Killworth (1985) and Winton (1996). A warm (light) anomaly at depth, located right at the eastern wall in stable stratification, leads to flow away from the wall (hence downwelling) at the northern rim of the anomaly and to flow toward the wall (hence upwelling) at the southern rim. In a stable stratification, the downwelling warms while the upwelling cools, leading to northward migration of the anomaly. In contrast, a cold (dense) anomaly in an *unstable* stratification at the eastern wall causes downwelling (hence *cooling*) at its southern rim and upwelling (hence *warming*) at its northern rim, which translates into southward migration of the anomaly.

For the case considered here, the image vortex and boundary wave descriptions lead to the same result; that is, the deep temperature anomalies propagate toward each other along the eastern wall. The two mechanisms are not equivalent, however; the vortex propagation describes the material motion (horizontal advection) of water with anomalous temperature, whereas the boundary wave propagation is associated with the adiabatic vertical displacement of isopycnals. The difference between the mechanisms shows up when other scenarios are considered. It is readily confirmed that in the boundary wave picture, the propagation direction along the eastern wall is independent of the sign of the anomaly (warm or cold) and only depends on the sign of the stratification (consistent with the notion of a linear wave). In contrast, the image vortex picture appears oblivious to whether a temperature anomaly exists in a stable or unstable stratification. While a closer investigation of which mechanism dominates here is beyond the scope of this paper, we conclude that there are at least two plausible candidate mechanisms for explaining why narrowness of deep sinking persists even under rotating three-dimensional dynamics.[5]

e. Concluding remarks

The model used here is relatively simple and crude, so perhaps the conclusions drawn from it are interesting possibilities rather than definitive answers. The main points are:

1. In the limit of very efficient convective mixing (in which the earth's ocean operates), the strength of the model's thermohaline circulation (THC) is insensitive to changes in convective mixing efficiency over orders of magnitude. This confirms the previous notion that diapycnal mixing and the surface density difference, but not convective mixing, limit the strength of the THC.

2. While convective mixing is central in setting deep-water properties, essentially to the temperature and salinity of the densest surface water, it is not required for vigorous buoyancy-driven overturning to exist. On the contrary, the strength of the meridional overturning increases in the model runs where the efficiency of convective mixing is reduced. In our numerical experiments, convective mixing appears to"drain" the system of potential energy, which causes the reduction in the THC. While it remains to be investigated whether this statement is generally valid, in our experiments the convective mixing does not provide energy to and hence does not "push" the large-scale flow.

3. Previous rationalizations of why deep sinking is narrow, which ostensibly rely on purely thermodynamical arguments, are incomplete since the models on which they are based all implicitly invoke two-dimensional dynamics. As one consequence of the two-dimensionality, downwelling and convective mixing are collocated, and the downwelling can often (but not always)[6] substitute for convective mixing as an efficient vertical transport agent. This tends to limit the importance of convective mixing in two-dimensional models (Zhang et al. 1992).

4. Under three-dimensional rotating dynamics, convective mixing and downwelling to the bottom are not necessarily collocated and hence may be clearly identifiable as very different processes. Convective mixing to the bottom occurs at the location of highest surface density, on a very small scale. Narrowness of downwelling likewise persists, but rotating, geostrophic dynamics must be invoked for the explanation. Convective mixing acts as a buoyancy sink to the deep ocean, while spatially integrated deep downwelling acts as a buoyancy source; such a balance suggests that vertical diffusion plays a negligible direct role in setting deep ocean properties.

Acknowledgments

We wish to thank Kerry Emanuel and Carl Wunsch for discussions and comments on an earlier version of the manuscript. Supported in part by NSF Grant OCE-9801800 and the U.S. Department of Energy through the Climate Change Prediction Program.

REFERENCES

Armi, L., 1978: Some evidence for boundary mixing in the deep ocean. *J. Geophys. Res.*, **83,** 1971–1979..

Bryan, F., 1987: Parameter sensitivity of primitive equation ocean general circulation models. *J. Phys. Oceanogr.*, **17,** 970–985.. Find this article online

Bryan, K., 1969: A numerical method for the study of the circulation of the world ocean. *J. Comput. Phys.*, **4,** 347–376..

— ,~~1~~984: Accelerating the convergence to equilibrium of ocean climate models. *J. Phys. Oceanogr.*, **14,** 666–673.. Find this article online

Cessi, P., and W. R. Young, 1992: Multiple equilibria in two-dimensional thermohaline circulation. *J. Fluid Mech.*, **241,** 291–309..

Colin de Verdière, A., 1988: Buoyancy driven planetary flows. *J. Mar. Res.*, **46,** 215–265.

Cox, M. D., 1984: A primitive equation, three-dimensional model of the ocean. GFDL Ocean Group Tech. Rep. No 1, GFDL/Princeton University. [Available from GFDL/NOAA, Princeton University, P.O. Box 308, Princeton, NJ 08542.].

Emanuel, K. A., J. D. Neelin, and C. S. Bretherton, 1994: On large-scale circulation in convecting atmospheres. *Quart. J. Roy. Meteor. Soc.*, **120,** 1111–1143..

Huang, R. X., 1998: Mixing and available potential energy in a Boussinesq ocean. *J. Phys. Oceanogr.*, **28,** 669–678.. Find this article online

Killworth, P. D., 1985: A two-level wind and buoyancy driven thermocline model. *J. Phys. Oceanogr.*, **15,** 1414–1432.. Find this article online

Klinger, B. A., and J. Marotzke, 1999: Behavior of double hemisphere thermohaline flows in a single basin. *J. Phys. Oceanogr.*, **29,** 382–399.. Find this article online

— ,~~J.~~ Marshall, and U. Send, 1996: Representation of convective plumes by vertical adjustment. *J. Geophys. Res.*, **101,** 18 175–18 182..

Kundu, P. K., 1990: *Fluid Mechanics.* Academic Press, 638 pp..

Macdonald, A. M., and C. Wunsch, 1996: An estimate of global ocean circulation and heat fluxes. *Nature*, **382,** 436–439..

Marotzke, J., 1989: Instabilities and multiple steady states of the thermohaline circulation. *Oceanic Circulation Models: Combining Data and Dynamics*, D.L.T. Anderson and J. Willebrand, Eds., NATO ASI Series, Kluwer Academic Press, 501–511..

— ,~~1~~991: Influence of convective adjustment on the stability of the thermohaline circulation. *J. Phys. Oceanogr.*, **21,** 903–907.. Find this article online

— ,~~1~~997: Boundary mixing and the dynamics of three-dimensional thermohaline circulations. *J. Phys. Oceanogr.*, **27,** 1713–1728.. Find this article online

— ,~~a~~nd B. A. Klinger, 2000: The dynamics of equatorially asymmetric thermohaline circulations. *J. Phys. Oceanogr.*, in press..

— ,~~P~~. Welander, and J. Willebrand, 1988: Instability and multiple steady states in a meridional-plane model of the thermohaline circulation. *Tellus*, **40A,** 162–172..

Marshall, J., and F. Schott, 1999: Open-ocean convection: Observations, theory and models. *Rev. Geophys.*, **37,** 1–64..

Munk, W., 1966: Abyssal recipes. *Deep-Sea Res.*, **13,** 707–730..

— ~~,~~ and C. Wunsch, 1998: Abyssal recipes II: Energetics of tidal and wind mixing. *Deep-Sea Res.*, **45,** 1977–2010..

Polzin, K. L., J. M. Toole, J. R. Ledwell, and R. W. Schmitt, 1997: Spatial variability of turbulent mixing in the abyssal ocean. *Science*, **276,** 93–96..

Quon, C., and M. Ghil, 1992: Multiple equilibria in thermosolutal convection due to salt-flux boundary conditions. *J. Fluid Mech.*, **245,** 449–483..

Rossby, H. T., 1965: On thermal convection driven by non-uniform heating from below: An experimental study. *Deep-Sea Res.*, **12,** 9–16..

Send, U., and J. Marshall, 1993: Integral effects of deep convection. *J. Phys. Oceanogr.*, **23,** 855–872.. Find this article online

Stommel, H., 1962: On the smallness of the sinking regions of the ocean. *Proc. Natl. Acad. Sci. USA*, **48,** 766–772..

Thual, O., and J. C. McWilliams, 1992: The catastrophe structure of thermohaline convection in a two-dimensional fluid model and a comparison with low-order box models. *Geophys. Astrophys. Fluid Dyn.*, **64,** 67–96..

Tziperman, E., 1997: Inherently unstable climate behavior due to weak thermohaline ocean circulation. *Nature*, **386,** 592–595..

Weyl, P. K., 1968: The role of the oceans in climate change: A theory of the ice ages. *Causes of Climate Change, Meteor. Monogr.*, No. 30, Amer. Meteor. Soc., 37–62..

Winton, M., 1995: Why is the deep sinking narrow? *J. Phys. Oceanogr.*, **25,** 997–1005.. Find this article online

— ~~,~~ 1996: The role of horizontal boundaries in parameter sensitivity and decadal-scale variability of coarse-resolution ocean general circulation models. *J. Phys. Oceanogr.*, **26,** 289–304.. Find this article online

Wright, D. G., and T. F. Stocker, 1991: A zonally averaged ocean model for the thermohaline circulation. Part I: Model development and flow dynamics. *J. Phys. Oceanogr.*, **21,** 1713–1724.. Find this article online

— ~~,~~ C. B. Vreugdenhil, and T. M. C. Hughes, 1995: Vorticity dynamics and zonally averaged ocean circulation models. *J. Phys. Oceanogr.*, **25,** 2141–2154. Find this article online

Wunsch, C., 1970: On oceanic boundary mixing. *Deep-Sea Res.*, **17,** 293–301..

Zhang, S., C. A. Lin, and R. J. Greatbatch, 1992: A thermocline model for ocean-climate studies. *J. Mar. Res.*, **50,** 99–124..

Figures

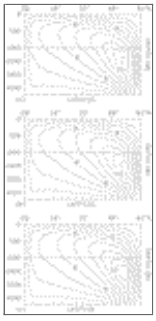

Click on thumbnail for full-sized image.

Fig. 1. Meridional overturning: contour interval is 2 Sv. The flow is such that high values are to the right, that is, clockwise around a high and anticlockwise around a low. (a) Expt 1, $k_c = 10\ \mathrm{m^2\ s^{-1}}$; (b) expt 2, $k_c = 1\ \mathrm{m^2\ s^{-1}}$; and (c) expt 3, $k_c = 0.1\ \mathrm{m^2\ s^{-1}}$.

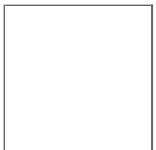

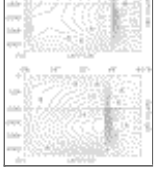

Click on thumbnail for full-sized image.

Fig. 2. Meridional overturning: contour interval is 2 Sv, negative values are dashed, and areas with negative values are shaded. The flow is such that high values are to the right, that is, clockwise around a high and anticlockwise around a low. (a) Expt 4, k_c = 100×10^{-4} m^2 s^{-1}; (b) expt 5, $k_c = 10 \times 10^{-4}$ m^2 s^{-1}; and (c) expt 6, $k_c = 5 \times 10^{-4}$ m^2 s^{-1}.

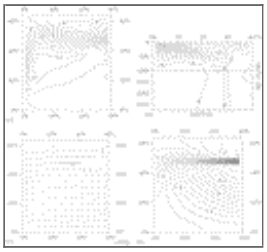

Click on thumbnail for full-sized image.

Fig. 3. Experiment 6, $k_c = 5 \times 10^{-4}$ m^2 s^{-1}: (a) Temperature at level 5 (425-m depth); contour interval is 0.5°C. (b) Temperature along the eastern wall; contour interval is 1°C. (c) Horizontal velocity at the lowest level (4250-m depth); reference arrow 5 cm s^{-1}; no arrows with speeds greater than 5 cm s^{-1} are plotted. (d) Temperature at the lowest level (4250-m depth); contour interval is 0.05°C. Notice that the coldest temperatures (less than 6.85°C) are at the eastern wall, just north of the front at about 48°N.

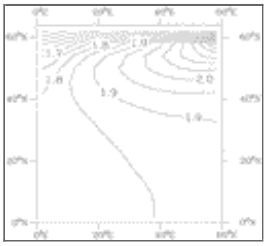

Click on thumbnail for full-sized image.

Fig. 4. Experiment 2, $k_c = 1$ m^2 s^{-1}: Temperature at the lowest level (4250-m depth); contour interval is 0.05°C.

[1] The available potential energy (APE) matters for the dynamics: how APE is influenced by convective activity is not obvious, although Huang (1998) concluded that APE was reduced.

[2] Marotzke (1991) employed different convective adjustment schemes and noted that they differed in their efficiency in removing static instability yet gave similar steady states when surface density was fixed. The comparison was not a clean one, however. Zhang et al. (1992) omitted convective adjustment altogether in one of their experiments but did not explore a range of convective efficiencies.

[3] By "efficient" convection we mean that convection occurs faster than any other important process in the model. The condition is easily fulfilled when convection is compared to the timescales of advection, diffusion, or internal Rossby waves. In the absence of variable wind forcing, external mode Rossby waves play no role. The interaction of convection with gravity waves and hence the geostrophic adjustment is distorted (Bryan 1984), but this process is already severely compromised by the asynchronous integration and not of interest here.

[4] We mean here the spatial extent of the region of deep mixing relative to the basin area. In two dimensions, this applies to the meridional extent only. In three dimensions (see section 4d), the eastern boundary blocks eastward flow, creating zonal convergence and zonally narrow downwelling there (e.g., Colin de Verdière 1988);the question of narrowness then again applies to the meridional extent.

[5] Notice that both mechanisms are ultimately based on simple geostrophic flow around a deep temperature anomaly. Since thermal wind is a good approximation even on the grid scale of the model, we expect the dynamical arguments to be qualitatively robust to changes in the model's resolution.

[6] Depending on the surface boundary conditions, the presence of convective mixing can be crucial even in two-dimensional models (e.g., Marotzke 1989).

Corresponding author address: Dr. Jochem Marotzke, Department of Earth, Atmospheric, and Planetary Science, Room 54-1514 Massachusetts

Institute of Technology, 77 Massachusetts Avenue, Cambridge, MA 02139.

E-mail: jochem@sound.mit.edu

top